

# Lawrence Berkeley National Laboratory

## LBL Publications

### Title

OzDES Reverberation Mapping Program: H $\beta$  lags from the 6-yr survey

### Permalink

<https://escholarship.org/uc/item/01s252kk>

### Journal

Monthly Notices of the Royal Astronomical Society, 520(2)

### ISSN

0035-8711

### Authors

Malik, U  
Sharp, R  
Penton, A  
[et al.](#)

### Publication Date

2023-02-07

### DOI

10.1093/mnras/stad145

### Copyright Information

This work is made available under the terms of a Creative Commons Attribution License, available at <https://creativecommons.org/licenses/by/4.0/>

Peer reviewed

# OzDES Reverberation Mapping Program: $H\beta$ lags from the 6-yr survey

U. Malik<sup>1</sup>,<sup>1\*</sup> R. Sharp,<sup>1\*</sup> A. Penton<sup>2</sup>, Z. Yu,<sup>3</sup> P. Martini,<sup>3,4,5</sup> C. Lidman<sup>1</sup>, B. E. Tucker,<sup>1,6,7</sup> T. M. Davis<sup>2</sup>, G. F. Lewis<sup>8</sup>, M. Agüena<sup>9</sup>, S. Allam,<sup>10</sup> O. Alves,<sup>11</sup> F. Andrade-Oliveira,<sup>11</sup> J. Asorey<sup>12</sup>, D. Bacon,<sup>13</sup> E. Bertin<sup>14,15</sup>, S. Bocquet,<sup>16</sup> D. Brooks,<sup>17</sup> D. L. Burke,<sup>18,19</sup> A. Carnero Rosell<sup>9,20,21</sup>, D. Carollo,<sup>22</sup> M. Carrasco Kind<sup>23,24</sup>, J. Carretero<sup>25</sup>, M. Costanzi,<sup>22,26,27</sup> L. N. da Costa,<sup>9</sup> M. E. S. Pereira,<sup>28</sup> J. De Vicente<sup>12</sup>, S. Desai,<sup>29</sup> H. T. Diehl,<sup>10</sup> P. Doel,<sup>17</sup> S. Everett,<sup>30</sup> I. Ferrero<sup>31</sup>, J. Frieman,<sup>10,32</sup> J. García-Bellido<sup>33</sup>, D. W. Gerdes,<sup>11,34</sup> D. Gruen<sup>16</sup>, R. A. Gruendl,<sup>23,24</sup> J. Gschwend,<sup>9,35</sup> S. R. Hinton<sup>2</sup>, D. L. Hollowood<sup>36</sup>, K. Honscheid,<sup>3,4</sup> D. J. James,<sup>37</sup> K. Kuehn,<sup>38,39</sup> J. L. Marshall,<sup>40</sup> J. Mena-Fernández,<sup>12</sup> F. Menanteau,<sup>23,24</sup> R. Miquel,<sup>25,41</sup> R. L. C. Ogando<sup>35</sup>, A. Palmese<sup>42</sup>, F. Paz-Chinchón,<sup>24,43</sup> A. Pieres<sup>35,44</sup>, A. A. Plazas Malagón<sup>45</sup>, M. Raveri,<sup>46</sup> M. Rodríguez-Monroy,<sup>12</sup> A. K. Romer,<sup>47</sup> E. Sanchez,<sup>12</sup> V. Scarpine,<sup>10</sup> I. Sevilla-Noarbe,<sup>12</sup> M. Smith<sup>48</sup>, M. Soares-Santos,<sup>11</sup> E. Suchyta<sup>49</sup>, M. E. C. Swanson,<sup>17</sup> G. Tarle,<sup>11</sup> G. Taylor<sup>1</sup>, D. L. Tucker,<sup>10</sup> N. Weaverdyck<sup>11,50</sup> and R.D. Wilkinson<sup>47</sup>

Affiliations are listed at the end of the paper

Accepted 2023 January 11. Received 2022 December 21; in original form 2022 October 10

## ABSTRACT

Reverberation mapping measurements have been used to constrain the relationship between the size of the broad-line region and luminosity of active galactic nuclei (AGN). This  $R-L$  relation is used to estimate single-epoch virial black hole masses, and has been proposed to use to standardize AGN to determine cosmological distances. We present reverberation measurements made with  $H\beta$  from the 6-yr Australian Dark Energy Survey (OzDES) Reverberation Mapping Program. We successfully recover reverberation lags for eight AGN at  $0.12 < z < 0.71$ , probing higher redshifts than the bulk of  $H\beta$  measurements made to date. Our fit to the  $R-L$  relation has a slope of  $\alpha = 0.41 \pm 0.03$  and an intrinsic scatter of  $\sigma = 0.23 \pm 0.02$  dex. The results from our multi-object spectroscopic survey are consistent with previous measurements made by dedicated source-by-source campaigns, and with the observed dependence on accretion rate. Future surveys, including LSST, TiDES, and SDSS-V, which will be revisiting some of our observed fields, will be able to build on the results of our first-generation multi-object reverberation mapping survey.

**Key words:** galaxies: active – galaxies: nuclei – quasars: emission lines – quasars: general – quasars: supermassive black holes.

## 1 INTRODUCTION

Reverberation mapping (RM) has been established as the leading technique for direct determination of black hole masses ( $M_{\text{BH}}$ ) in active galactic nuclei (AGN) outside the local universe. Reverberation measurements anchor the scaling relations used to estimate single-epoch virial black hole (BH) masses (Vestergaard 2002; Vestergaard & Peterson 2006). Over the past decade, RM programs conducted by the Australian Dark Energy Survey (OzDES) and Sloan Digital Sky Survey (SDSS) have leveraged high-multiplexed spectroscopy to perform RM on an ‘industrial’ scale, aiming to increase the number of measurements available by an order of magnitude (King et al. 2015; Shen et al. 2015). These programs have resulted in over one hundred new lag measurements, while also identifying and addressing the complexities of performing RM on such large scales.

As reverberation mapping resolves the innermost regions of AGN in the time-domain, rather than spatially, it allows the study of these regions out to high redshifts. RM utilizes the difference in the light travel time between the variation of the continuum emission from the accretion disc around the central supermassive black hole (SMBH) and the reprocessed emission from the photoionized broad-line region (BLR; Blandford & McKee 1982; Peterson 1993). The time-delay,  $\tau$ , can be measured using multi-epoch photometry and spectroscopy to probe the continuum and BLR response, respectively, in order to infer the radius of the BLR ( $R_{\text{BLR}} = c\tau$ ). Together with the BLR velocity dispersion,  $\Delta V^2$ , inferred from the width of the emission line, this can be used to estimate the mass of the SMBH using the virial product:

$$M_{\text{BH}} = f \frac{R_{\text{BLR}} \Delta V^2}{G}. \quad (1)$$

The geometry, orientation, and kinematics of the BLR are encapsulated by the dimensionless scale factor  $f$ , which is calibrated using

\* E-mail: [Umang.Malik@anu.edu.au](mailto:Umang.Malik@anu.edu.au) (UM); [rob.sharp@anu.edu.au](mailto:rob.sharp@anu.edu.au) (RP)

sources with independent measurements from RM and the  $M_{\text{BH}}-\sigma_*$  relation (Ferrarese & Merritt 2000; Gebhardt et al. 2000; Onken et al. 2004; Woo et al. 2015).

Due to the intensity of observational resources required, early programs targeted a small number of local AGN with campaign durations of less than 1 yr. To achieve the fidelity required for RM, they observed bright, highly varying AGN. As a result, the targeted samples are typically biased towards AGN in the local universe ( $z < 0.3$ ). Lag measurements were made for 63 AGN with the  $H\beta$  line (e.g. Peterson et al. 1998; Kaspi et al. 2000; Peterson & Horne 2004; Bentz et al. 2009). These measurements were used to constrain the relationship between the AGN luminosity and the radius of the BLR ( $R-L$  relation), which exhibited relatively low intrinsic scatter, with a slope consistent with that expected by photoionization physics (Bentz et al. 2009, 2013). This relation calibrates secondary mass-scaling relations used to estimate single-epoch virial BH masses for samples of thousands of AGN (e.g. SDSS DR7 quasar catalogue, Shen et al. 2011). The  $R-L$  relation has also been proposed as a way to standardize AGN for use as luminosity distance indicators for cosmology (Watson et al. 2011; Martínez-Aldama et al. 2019; Khadka et al. 2022).

These BH mass estimates have a significant  $\sim 0.5$  dex uncertainty due to our limited understanding of BLR geometry and kinematics, and the small sample of reverberation measurements among other factors (Shen 2013). The former issue is addressed by conducting observationally intensive velocity-resolved RM (e.g. Bentz et al. 2010; Grier et al. 2013; Pancoast et al. 2014b; Du et al. 2018; U et al. 2022), and using dynamical modelling methods (e.g. CAMEL, Pancoast, Brewer & Treu 2014a), as well as spectroastrometry of the BLR in local AGN (e.g. GRAVITY, Gravity Collaboration et al. 2018). Other programs are targeting a more diverse range of sources. The super-Eddington accreting massive black holes (SEAMBH) program has observed over 40 luminous AGN (Du et al. 2014; Wang et al. 2014; Du et al. 2015, 2016, 2018; Hu et al. 2021). The updated  $R-L$  relation using these  $H\beta$  measurements has increased intrinsic scatter, and an observed dependence on accretion rate. However, these programs are still only targeting AGN at  $z < 0.4$ .

The SDSS-RM Project and our OzDES-RM program have pioneered RM on an ‘industrial-scale’, observing hundreds of AGN probing a wide range of AGN luminosities and redshifts. These programs have added over 100 new lag measurements, and have enabled the  $\text{MgII}$  and  $\text{CIV}$   $R-L$  relations to be constrained with statistically significant samples (Grier et al. 2017; Grier et al. 2019; Hoormann et al. 2019; Homayouni et al. 2020; Yu et al. 2021, 2022, Penton et al. in prep). The first generation of multi-object RM surveys have however highlighted problems with monitoring hundreds of targets. This includes challenges both with data quality (signal to noise, limited temporal coverage; Malik et al. 2022) as well as with reverberation lag recovery techniques and biases such as aliasing (Li et al. 2019; Penton et al. 2022).

OzDES focused mainly on high-redshift AGN; however, about 10 per cent of the sample contains  $H\beta$  emission within the spectroscopic window. This will allow comparison of our OzDES measurements with the large sample of existing  $H\beta$  measurements, in order to examine the consistency of multi-object RM with earlier dedicated source-by-source observations. We present the  $H\beta$  lag results from our 6-yr survey. Section 2 details the observations obtained by OzDES and the data calibration procedures. In Section 3, we describe the techniques we used for lag recovery and the selection criteria we apply to define our final sample. In Section 4, we present our successful lag measurements and black hole masses, as well as an updated  $R-L$  relationship, and discuss these results in Section 5.

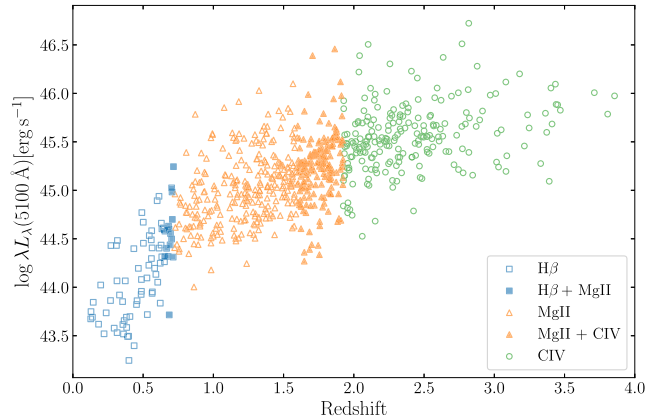


**Figure 1.** Distribution of redshifts and monochromatic luminosities at 5100 Å for the 735 AGN in the OzDES RM sample. The  $H\beta$  sample extends to  $z = 0.75$ , with 15 sources overlapping with our  $\text{MgII}$  sample.

We summarize our results and then present an outlook for the future work in Section 6. Throughout this work we adopt a flat  $\Lambda$ CDM cosmology with  $\Omega_\Lambda = 0.7$ ,  $\Omega_M = 0.3$ , and  $H_0 = 70 \text{ km s}^{-1} \text{ Mpc}^{-1}$ .

## 2 DATA

The Australian Dark Energy Survey (OzDES) provided follow-up spectroscopic observations of the 10 supernova fields observed by the DES. The DES supernova fields are located in the ELAIS, *XMM*-Large-Scale Structure, *Chandra* deep-field South, and SDSS Stripe 82 regions (Kessler et al. 2015; Morganson et al. 2018). These fields were observed in the *griz* filters with the Dark Energy Camera (DECam) on the 4-m Blanco telescope at Cerro Tololo Inter-American Observatory (CTIO) (Flaugher et al. 2015). From 2013 to early 2018, the fields were observed with  $\sim 6$  d cadence over a 5–6 month season (August to January), with additional science verification data taken in late 2012 to early 2013, and additional data taken on a monthly cadence in late 2018. OzDES conducted follow-up multi-object spectroscopic observations with the 2dF multi-object fibre positioning system and the AAOmega spectrograph (3700–8800 Å, Sharp et al. 2006) on the 3.9-m Anglo-Australian Telescope (AAT; Yuan et al. 2015; Childress et al. 2017; Lidman et al. 2020). The OzDES observations were made over the same 5–6 month season with approximately monthly cadence from 2013 to 2019.

### 2.1 Target sample

After completing the final data reduction for our survey, the OzDES RM Program sample comprises 735 AGN (reduced from an initial sample of 771 due to a change in the location of the DECam inter-chip gaps between survey definition and campaign observations), with redshifts ranging up to  $z \sim 4$ , and with apparent magnitudes  $17.2 < r_{\text{AB}} < 22.3$  mag. The redshift and luminosity distribution of these AGN is shown in Fig. 1.

Of these 735 AGN, the  $H\beta$  line and nearby continuum falls within the AAOmega spectral range for 78 sources. The expected observer-frame lags for the  $H\beta$  sample (governed by luminosity and time-dilation) range from  $\sim 20$  d to just over 200 d. In previous analyses, our emission-line flux measurements were made using spectra that were co-added by observing run (Hoormann et al. 2019) (typically 4–7 d during dark time each month). However, some fields were observed over multiple nights within a single observing run. To maximize the cadence of our sampling we treated the spectra

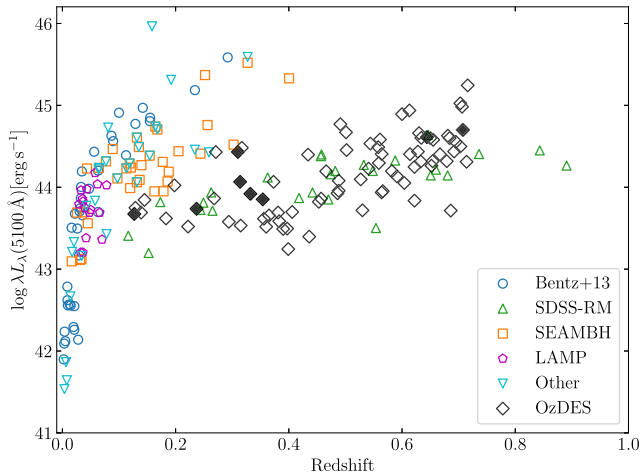


**Figure 2.** The redshift and luminosity distribution for the OzDES H $\beta$  sample (open diamonds), final sample (filled diamonds, see Section 4), and existing measurements from Bentz et al. (2013, and references therein); SDSS-RM (Grier et al. 2017, quality 4 and 5); SEAMBH (Du et al. 2014; Wang et al. 2014; Du et al. 2015, 2016, 2018; Hu et al. 2021); Lick AGN Monitoring Project (LAMP, U et al. 2022); and other measurements from Bentz et al. (2009), Barth et al. (2013), Bentz et al. (2014), Pei et al. (2014), Lu et al. (2016), Bentz et al. (2016a), Bentz et al. (2016b), Fausnaugh et al. (2017), Zhang et al. (2019), Rakshit et al. (2019), Li et al. (2021), of which measurements published before 2019 are compiled by Martínez-Aldama et al. (2019).

obtained on different nights as separate epochs for our emission-line light curves. This is particularly valuable for rapidly reverberating sources. The redshift and luminosity range of our H $\beta$  sample, and H $\beta$  measurements from the literature are shown in Fig. 2.

We do not measure the continuum luminosity directly from the spectra due to fibre aperture effects from variable atmospheric seeing and fibre placement uncertainties. From the average  $r$ -band magnitude and redshift of the AGN, we estimated the monochromatic continuum flux at 5100 Å using the DECam  $r$ -band filter transmission curve and the SDSS quasar template (Vanden Berk et al. 2001). The template is scaled to the magnitude of the source, assuming  $L_{\text{bol}} = 9 \lambda L_{\lambda}(5100 \text{ \AA})$  (Kaspi et al. 2000).

## 2.2 Flux calibration and measurements

The DES photometry is calibrated consistently through to Y6 using the DES data reduction pipeline (Burke et al. 2018; Morganson et al. 2018). We perform a spectrophotometric flux calibration and line flux measurement following Hoormann et al. (2019). The local continuum windows for continuum subtraction are 4760 to 4790 Å and 5100 to 5130 Å. The calibration uncertainties of the line flux were measured using the F-star warping function method as detailed in Yu et al. (2021).

## 3 LAG RECOVERY AND RELIABILITY

### 3.1 Time series analysis

To measure the reverberation lags for our sample we use the interpolated cross-correlation function (ICCF; Gaskell & Peterson 1987) and JAVELIN (Zu, Kochanek & Peterson 2011; Zu et al. 2013) methodologies. The JAVELIN method models the AGN continuum variability using a damped random walk (DRW; Kelly, Bechtold & Siemiginowska 2009; Kozłowski et al. 2010; MacLeod

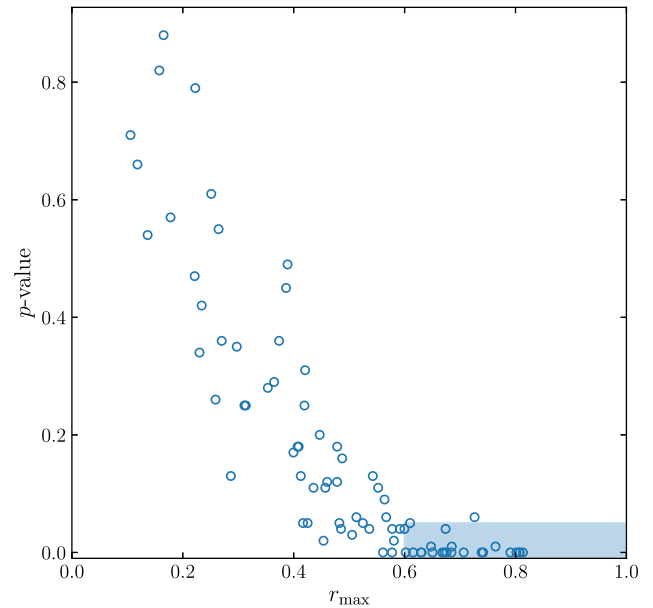


**Figure 3.**  $p$ -value versus  $r_{\text{max}}$  for our 78 AGN. The  $r_{\text{max}}$  is of the original pair of light curves. The shaded region indicates our selection criteria requiring a  $p$ -value  $< 0.05$  and  $r_{\text{max}} > 0.6$ .

et al. 2010). It assumes the emission-line light curve is a scaled, smoothed, and shifted version of the continuum light curve that can be described by the convolution of the continuum with a top-hat transfer function. Using Markov Chain Monte Carlo (MCMC), it constrains the characteristic variability amplitude and damping time-scale of the continuum light curve. Applying this DRW fit as a prior, it simultaneously fits both the continuum and emission-line light curves, to derive the posterior distributions of the transfer function parameters: lag, top-hat width, and scale factor, as well as an updated DRW amplitude and time-scale. We allow these parameters to vary freely, while setting a lag prior of  $[-3\tau_{\text{exp}}, 3\tau_{\text{exp}}]$ , where  $\tau_{\text{exp}}$  is the expected H $\beta$  lag for the source using the Bentz et al. (2013)  $R$ - $L$  relation.

We use the PyCCF code to perform the ICCF method (Sun, Grier & Peterson 2018). This linearly interpolates the continuum and emission-line light curves over a user defined grid spacing, and cross-correlates the interpolated light curves as a function of time-lag. The centroid of the cross-correlation function (CCF) is computed as the median of the CCF values  $> 0.8r_{\text{max}}$  counted out from the peak of the CCF,  $r_{\text{max}}$ . A cross-correlation centroid distribution (CCCD) is obtained from 10 000 Monte Carlo realizations of the flux randomization and random subset sampling (FR/RSS) process (Peterson et al. 1998), which accounts for the flux measurement uncertainties and potentially spurious correlations between light-curve points. Following Hoormann et al. (2019), we set the interpolation grid spacing to 3 d, and the  $r_{\text{max}}$  threshold to 0.5. We use the same lag prior as for JAVELIN from  $[-3\tau_{\text{exp}}, 3\tau_{\text{exp}}]$ .

The recovered lag,  $\tau$ , with lower and upper uncertainties,  $\sigma_{\tau}$ , are taken to be median and 16th and 84th percentiles of the lag probability distribution functions (PDF) from JAVELIN and PyCCF.

### 3.2 Null hypothesis test

Our survey window function for the (expected) short H $\beta$  lags is less than ideal and the signal to noise of the spectroscopy is only modest. We wish to test the null hypothesis that our lag recovery

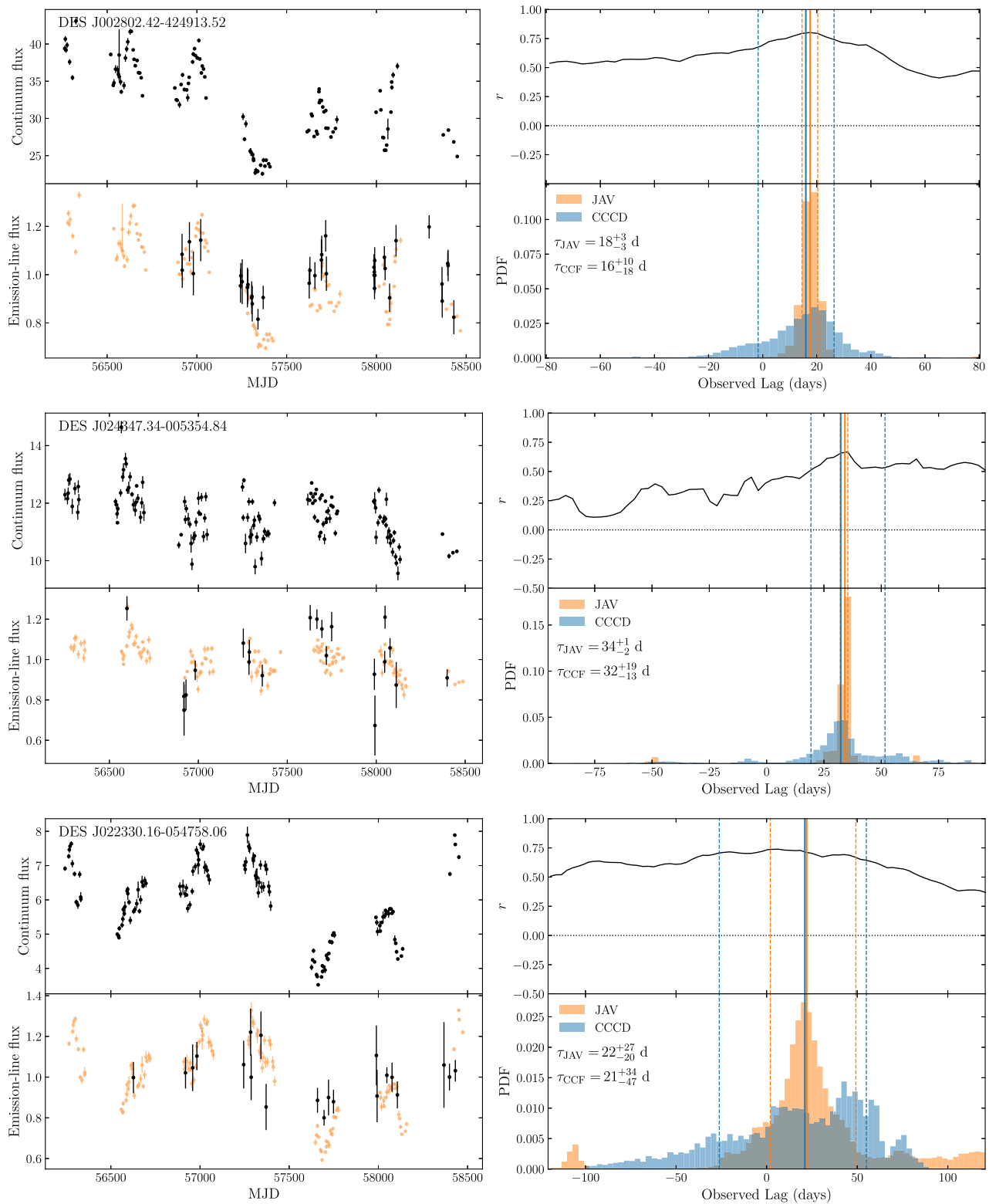


**Figure 4.** For each source, the upper-left-hand panel shows the DECam  $g$ -band continuum light curve, and lower-left-hand panel the  $H\beta$  emission-line light curve, with the continuum light curve phase-shifted by the JAVELIN lag. The fluxes have been re-scaled. The upper-right-hand panel shows the cross-correlation function computed using PYCCF. The lower-right-hand panel shows the cross-correlation centroid distribution (CCCD) from PYCCF in blue, and the lag posterior from JAVELIN in orange, with the vertical solid and dashed lines indicating the recovered lag and upper and lower uncertainties from each method.

is not simply a product of the interaction of the window function with underlying red-noise correlation in the photometric light curves (an underlying assumption of any RM technique). Therefore, we do not report extensive light-curve simulations of the H $\beta$  sample (as per U et al. 2022), as this would simply reuse the same window function properties with the added uncertainty of the appropriateness of the variability model for our sources. Instead we randomized the spectroscopic light curves (with flux values shuffled while retaining the dates of observation), and cross correlated this with the original photometric light curve. We find the  $r_{\max}$  value of the cross-correlation coefficient  $r$  at the peak of the CCF, and compare it to that found from the CCF of the original light curves. After 1000 iterations, the  $p$ -value was calculated as the fraction of  $r_{\max}$  values which exceeded the original  $r_{\max}$ .

By randomizing the emission-line light curves, we generate uncorrelated light curves that do not possess a reverberation signature. We chose to randomize the observed spectroscopic light curve, rather than using simulated light-curve realizations, as done by U et al. (2022). Simulated light-curve realizations have the same variability time-scale and underlying lag as the source, and therefore may result in significant spurious correlations at random lag values.

Fig. 3 shows the results of this test applied to each of the H $\beta$  sources. We see that below a  $r_{\max}$  of 0.6, there are always a significant number of uncorrelated signals which exceed this  $r_{\max}$ , resulting in high  $p$ -values. Therefore, we can not trust a result which has a  $r_{\max}$  below 0.6.

### 3.3 Selection criteria

Based on the results of simulations from Li et al. (2019), Yu et al. (2020), and Penton et al. (2022), we adopt the lag and uncertainties from JAVELIN as the final lag. We define a successful lag recovery as meeting the following criteria:

- (i) The upper and lower lag uncertainties  $\sigma_{\tau, \text{JAV}}$  are less than  $|\tau_{\text{JAV}}|$ , or 30 d, whichever is greater
- (ii)  $\tau_{\text{PyCCF}}$  lies within the  $2\sigma_{\tau, \text{JAV}}$  uncertainties
- (iii)  $p$ -value  $< 0.05$  and  $r_{\max} > 0.6$

As the expected lags of our sources range from  $\sim 20$  to 200 d, we use a relative rather than absolute cut on the lag uncertainties. We require the lags recovered from JAVELIN and PyCCF to agree in an attempt to exclude cases where PDF's are flat or have significant aliasing peaks. Our  $p$ -test and  $r_{\max}$  criteria ensure there is significant correlation between the light curves that is unlikely to be spurious.

## 4 RESULTS

We successfully measure lags for five H $\beta$  sources with the criteria listed in Section 3.3. The recovered lags are given in Table 1. We present the light curves and the lag distributions for each of the five sources in Figs 4 and 5. The re-scaled and phase-shifted light curves for each of the sources display visually discernible reverberation. For each source, there is overlap between the phase-shifted light curves. In most cases, the lag PDF's from PyCCF and JAVELIN agree, although there is significant scatter in the PyCCF CCFD's for some sources. However, even for these cases, the JAVELIN lag is well defined, which is consistent with the finding that JAVELIN is better able to recover short lags than PyCCF (Li et al. 2019).

### 4.1 Additional sources

After visually inspecting the lag recoveries from our full H $\beta$  sample, we identified eight sources with lag PDF's of comparable quality to the sample that passed our selection criteria, but with JAVELIN aliasing peaks. This signal is produced as an artefact of the survey window function; predominantly the seasonal gaps. These aliasing peaks do not coincide with a peak in the PyCCF CCFD or CCF, and always occur at negative lags coincident with the seasonal gaps in the observational campaign ( $\sim -150$  to  $-250$  d). We show the light curves and lag PDF's of these sources in Figs 6, A1, and A2. For most sources, there is good agreement in the light curves phase-shifted by the positive recovered lag. For three of the eight sources (Fig. 6), there is an overlap between the photometric and spectroscopic observations, while the light curves for the other five (Figs A1 and A2) shift such that the spectroscopic observations fall wholly within gaps in the photometric observations. For comparison, we phase-shifted the continuum light curve by the lag at which the negative JAVELIN peak occurs. We show the light curves phase-shifted by both the positive lag and the negative lag in Figs A3 and A4. In some cases, the light curves show smooth multiyear variations, for which the negatively phase-shifted light curves do seem to reasonably interpolate between the seasonal gaps; however, there is no coincident peak in the PyCCF CCFD.

If we omit the negative peaks in the JAVELIN PDF's, five of the eight sources pass our selection criteria, and therefore illustrate comparable quality to the sample recovered originally. Given there is no physical motivation for a negative reverberation lag, and the negative aliasing peaks seem to be an artefact of the JAVELIN method alone, we choose to include the three sources that demonstrate overlap between their light curves when shifted by the positive lag in our final sample. We provide the lags for these three sources in Table 1. At this stage, we choose not to include the other two sources, DES J024533.65-000744.91 and DES J004009.06-431255.29, which have positive lags that cause the phase-shifted light curves to land completely within the seasonal gaps. The three sources that do not pass all our selection criteria only fail the  $r_{\max}$  criterion, although we note that their  $r_{\max}$  are above 0.5. The phase-shifted light curves for these three sources also fall within the seasonal gaps. High cadence monitoring to resolve shorter term variations, and observing over longer seasons will be required to reliably recover these lags.

Fig. 2 shows the redshift and luminosity distribution of our final recovered sample of eight AGN, compared with existing measurements. Our sample probes higher redshifts, and spans 1 dex in luminosity.

### 4.2 Black hole masses and the $R$ - $L$ relation

We measured the H $\beta$  line-width using the line dispersion of the mean spectra. Although H $\beta$  line-width measurements are commonly made using the root mean squared (rms) spectra, the signal to noise of our spectra are insufficient to support this approach. We measure  $M_{\text{BH}}$  for our final sample of eight AGN using equation (1) and a virial factor  $f = 4.47$  (Woo et al. 2015), and give these in Table 1, along with the line dispersion measurements.

We constrain the  $R$ - $L$  relation as shown in Fig. 7. Our best fit to the existing data and our final sample is

$$\log(R_{\text{BLR}}/\text{lt} - \text{day}) = K + \alpha \log(\lambda L_{\lambda})/10^{44} [\text{erg s}^{-1}] \quad (2)$$

with slope  $\alpha = 0.41 \pm 0.03$ ,  $K = 1.33 \pm 0.02$ , and an intrinsic scatter of  $\sigma = 0.23 \pm 0.02$  dex.

**Table 1.** Results for our final sample of eight AGN. Columns left to right: DES name (J2000), redshift, observer-frame JAVELIN lag, observer-frame PyCCF lag,  $p$ -value, monochromatic luminosity at 5100Å, line dispersion measured from mean spectrum, virial black hole mass, and dimensionless accretion rate.

Source	$z$	$\tau_{\text{JAV}}$ (d)	$\tau_{\text{PyCCF}}$ (d)	$p$ -value	$\log(\lambda L_{5100})$ ( $\text{erg s}^{-1}$ )	$\sigma_{\text{mean}}$ ( $\text{km s}^{-1}$ )	$M_{\text{BH}}$ ( $\times 10^7 M_{\odot}$ )	$\dot{M}$
DES J002802.42-424913.52	0.127	$18^{+3}_{-3}$	$16^{+10}_{-18}$	0.000	43.67	$1393 \pm 3$	$2.64^{+0.85}_{-0.87}$	1.43
DES J024347.34-005354.84	0.237	$34^{+1}_{-2}$	$32^{+19}_{-13}$	0.000	43.74	$1658 \pm 6$	$6.62^{+1.87}_{-1.89}$	0.28
DES J022330.16-054758.06	0.354	$22^{+27}_{-20}$	$21^{+34}_{-47}$	0.002	43.85	$1846 \pm 11$	$4.86^{+6.12}_{-4.62}$	0.79
DES J002904.43-425243.04	0.644	$98^{+27}_{-57}$	$87^{+31}_{-177}$	0.002	44.61	$1851 \pm 4$	$17.8^{+7.0}_{-11.4}$	0.80
DES J022617.85-043108.99	0.707	$67^{+49}_{-18}$	$33^{+73}_{-80}$	0.006	44.70	$1691 \pm 8$	$9.78^{+7.60}_{-3.76}$	3.63
DES J034028.46-292902.41	0.310	$51^{+9}_{-6}$	$54^{+24}_{-22}$	0.002	44.43	$1732 \pm 5$	$10.3^{+3.3}_{-3.1}$	1.30
DES J022249.67-051453.01	0.314	$25^{+7}_{-5}$	$29^{+45}_{-55}$	0.005	44.07	$1883 \pm 5$	$5.99^{+2.28}_{-2.00}$	1.08
DES J003954.13-440509.97	0.332	$48^{+12}_{-7}$	$56^{+17}_{-37}$	0.001	43.92	$1856 \pm 11$	$10.9^{+4.1}_{-3.4}$	0.20

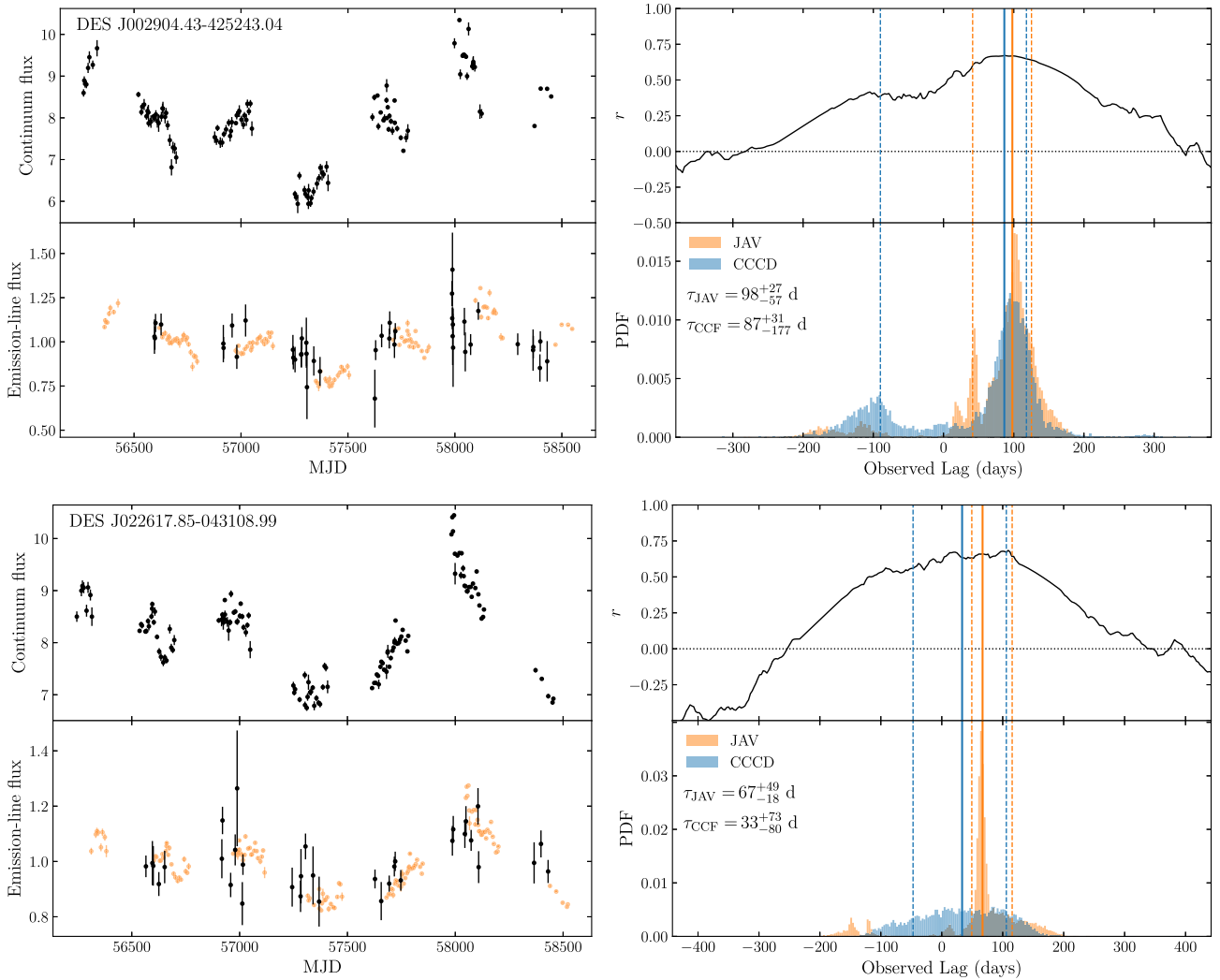


**Figure 5.** Same as for Fig. 4.

The SEAMBH program targeted highly accreting AGN at  $z < 0.4$  (Du et al. 2014; Wang et al. 2014; Du et al. 2015, 2016, 2018; Hu et al. 2021). SEAMBH found that highly accreting AGN have systematically shorter reverberation lags. They proposed that

accretion rate explains the observed deviation from the steeper  $R-L$  relation from the Bentz et al. (2013) compilation of earlier results. Following Du et al. (2018), we measure the dimensionless accretion rate of our sample using the estimator derived from the standard thin

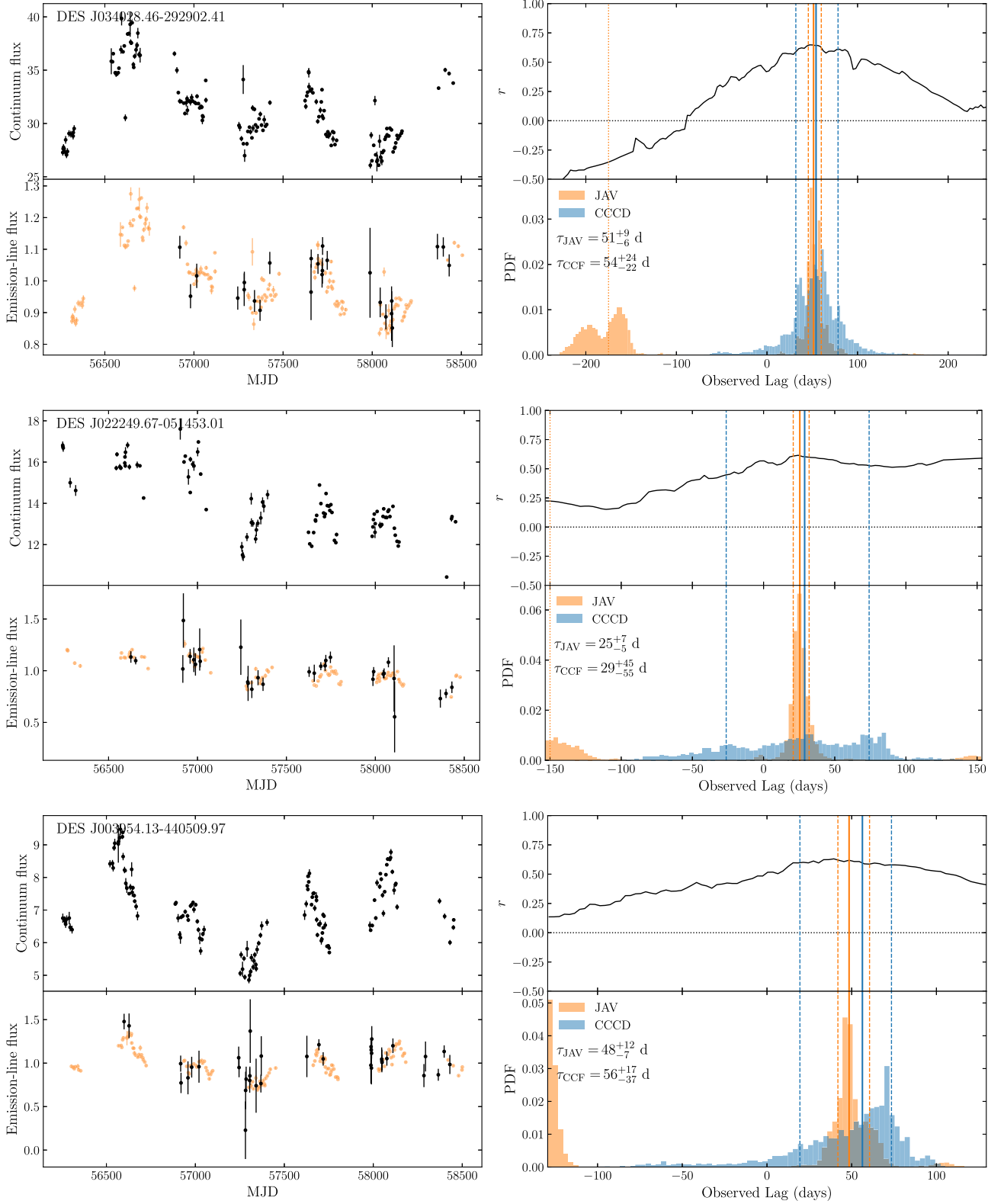


**Figure 6.** Same as for Fig. 4, for sources with JAVELIN aliasing signals. The orange vertical dotted lines indicate the negative aliasing peak in the JAVELIN PDF, for which we show the phase-shifted light curves in Appendix A. These three sources are included in the final sample.

accretion disc model (Shakura & Sunyaev 1973):

$$\dot{M} = 20.1 \left( \frac{l_{44}}{\cos(i)} \right)^{3/2} m_7^{-2}, \quad (3)$$

where  $l_{44} = L_{5100}/10^{44}$  erg  $s^{-1}$ ,  $m_7 = M_{\text{BH}}/10^7 M_{\odot}$ , and the inclination angle of the disc to the line of sight is taken to be  $\cos(i) = 0.75$ . All but one of our sources have low accretion rates, which is consistent



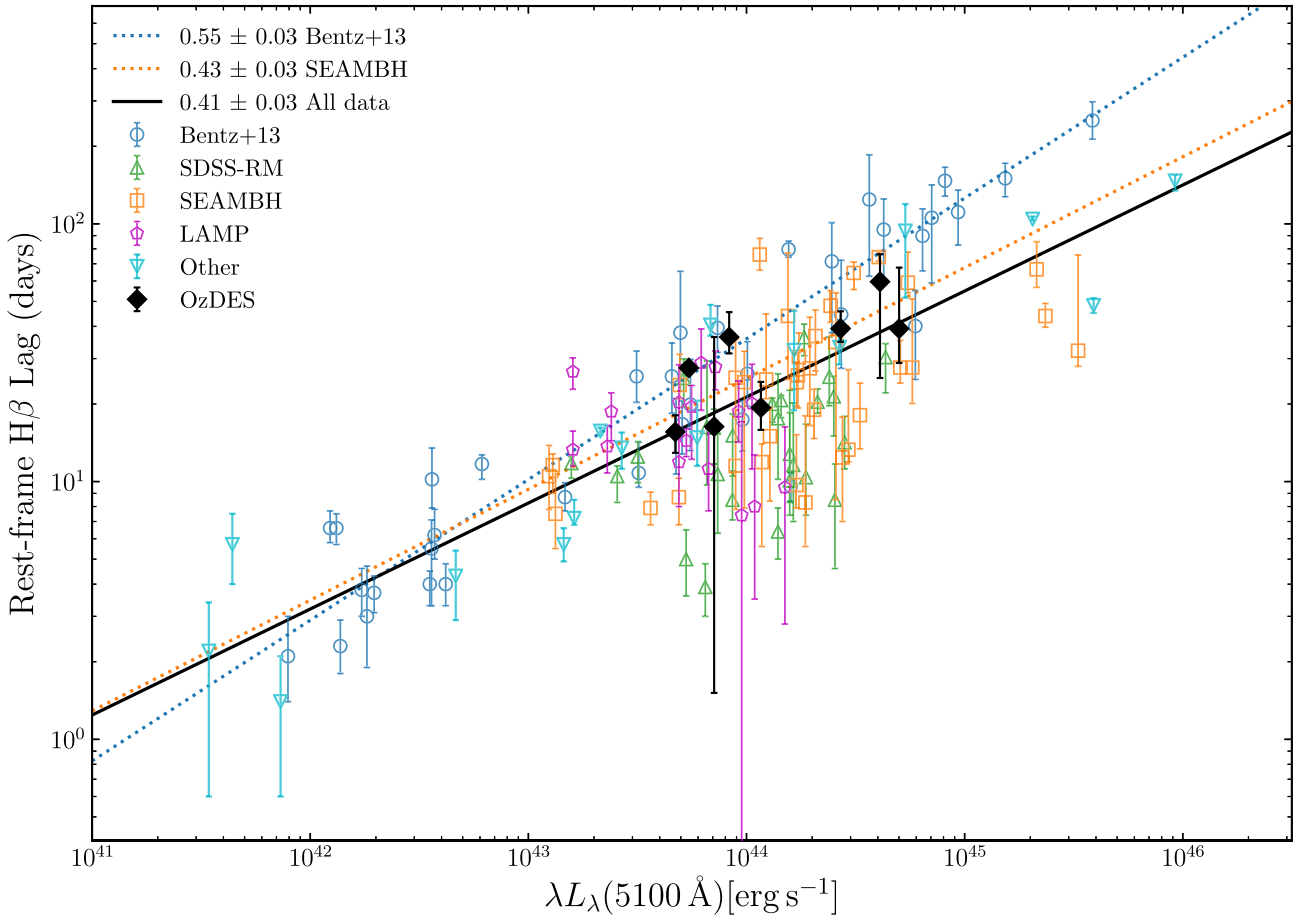


**Figure 7.** Radius–luminosity relation for  $H\beta$  using our final sample of eight new AGN together with existing measurements from Bentz et al. (2013, and references therein); SDSS-RM (Grier et al. 2017, quality 4 and 5); SEAMBH (Du et al. 2014; Wang et al. 2014; Du et al. 2015, 2016, 2018; Hu et al. 2021); Lick AGN Monitoring Project (LAMP, U et al. 2022); and other measurements from Bentz et al. (2009), Barth et al. (2013), Bentz et al. (2014), Pei et al. (2014), Lu et al. (2016), Bentz et al. (2016a), Bentz et al. (2016b), Fausnaugh et al. (2017), Zhang et al. (2019), Rakshit et al. (2019), Li et al. (2021), of which measurements published before 2019 are compiled by Martínez-Aldama et al. (2019). The slope of the relation is given in the legend, along with the slopes constrained previously by Bentz et al. (2013) and Du et al. (2018). All sources in the OzDES sample have low accretion rates, apart from our highest luminosity measurement (right-most black point), which has a moderately high accretion rate (Table 1).

with the observed agreement between our results and the Bentz et al. (2013) relation, which was constrained using mainly low-accretion sources. One of our sources is on the lower boundary of what SEAMBH define to be highly accreting, and is consistent with both the low-accretion and high-accretion samples.

## 5 DISCUSSION

The primary goal of the OzDES RM program was to make RM measurements at high redshifts, with the Mg II and C IV lines. Our monthly cadence was sufficient for this, due to the intrinsically longer reverberation lags for these high ionization lines, and the increased time dilation for such sources that are typically at higher redshifts than our  $H\beta$  sample. Simulations showed the OzDES observational cadence was likely insufficient to provide a full sample of  $H\beta$  RM measurements (King et al. 2015; Malik et al. 2022). Since our survey is not as sensitive to these shorter lags, some of our selection criteria are not as strict as other analyses. Some of the uncertainties on the lags we have recovered are considerably larger than previous works, as we lack the temporal resolution to recover lags precisely.

Our new measurements are more consistent with the Bentz et al. (2013) slope than the SDSS-RM  $H\beta$  sample (Grier et al. 2017),

although our sample has a similar redshift–luminosity distribution to SDSS-RM. As discussed by Grier et al. (2017), the SDSS-RM lags may underestimate  $M_{\text{BH}}$  due to selection effects from having only a single campaign season of observation, which limits the lag search window to 100 d. Our OzDES analysis is based on a 7 yr of photometry and 6 yr of spectroscopy but with lower observational cadence. However, simulations by Fonseca Alvarez et al. (2020) suggest this deviation is not due to observational biases. They attribute the deviation of their sample to changes in the UV/optical spectral energy distribution (SED), although this was not measured directly. The only significant difference between the OzDES and SDSS-RM samples and lag analyses is the baseline and cadence of the light-curve data.

Simulations presented by Malik et al. (2022) modelled survey window functions for OzDES and upcoming surveys, and investigated lag recovery efficacy with degraded or increased sampling. They find that with low sampling the scatter in the recovered  $R-L$  relation is increased, however there is no systematic offset from the input slope (see Fig. 13 in Malik et al. 2022). For sources with shorter expected lags and with a less-than-ideal cadence, they did not systematically recover longer lags. In the case that these idealized simulations are not representative of the data, it is possible that

with our cadence we may not be as sensitive to shorter lags if they were present. Upcoming surveys, including the Time-Domain Extragalactic Survey (TiDES; Swann et al. 2019) and SDSS-V Black Hole Mapper (Kollmeier et al. 2017), which will be spectroscopically following up the Legacy Survey of Space and Time (LSST) deep-drilling fields, will be revisiting most of the OzDES fields with shorter spectroscopic cadence. These programs can investigate any potential discrepancies with our results due to the longer cadence of OzDES.

## 6 SUMMARY

We successfully recover reverberation lags with H $\beta$  for eight AGN from the 6-yr observations from DES and OzDES. These results from our multi-object survey are consistent with previous H $\beta$  analyses done with source-by-source observations, including the early results compiled in Bentz et al. (2013). Our observations seem inconsistent with the large scatter observed in the SDSS-RM H $\beta$  sample (Grier et al. 2017), although the only significant difference between our analyses is the baseline and cadence of the survey data. Our sample includes only one moderately high accretion rate source, and the location of our final sample on the  $R-L$  relation is consistent with earlier measurements with similar source accretion rates. This work compliments the higher redshift results for the rest of the OzDES RM sample of 735 AGN, made with the Mg II (Yu et al. 2021, 2022) and C IV lines (Hoormann et al. 2019; Penton et al. 2022, Penton et al. in prep), which will be used to recalibrate black hole mass-scaling relations for those emission lines.

The H $\beta$  sample is highly sensitive to the observational window function. Additional campaign seasons seem to help, but higher cadence and observing over longer seasons is necessary to reliably recover these lags. Future surveys, including TiDES (Swann et al. 2019) and SDSS-V BHM (Kollmeier et al. 2017), which will be following up LSST, will observe some of the same fields as OzDES. These surveys can follow up with a more suitable window function (Malik et al. 2022). In order to anchor the ends of the H $\beta$   $R-L$  relation, future programs will need to target lower luminosity sources at  $10^{41} < \lambda L_{\lambda}(5100 \text{ \AA}) < 10^{43} \text{ ergs s}^{-1}$ , and higher luminosity sources at  $\lambda L_{\lambda}(5100 \text{ \AA}) > 10^{45} \text{ ergs s}^{-1}$ . The challenge is to have a survey area large enough to observe local sources at low luminosity, and the rare local high-luminosity sources. This is especially difficult for multi-object RM surveys, but by extending spectral coverage into the red-optical and infra-red range, such surveys can access the greater volume for such sources at higher redshifts with H $\beta$ .

## ACKNOWLEDGEMENTS

We thank the anonymous referee for their comments that improved the paper. UM and AP are supported by the Australian Government Research Training Program (RTP) Scholarship. PM and ZY were supported in part by the United States National Science Foundation under Grant No. 161553 to PM. PM is grateful for support from the Radcliffe Institute for Advanced Study at Harvard University. PM also acknowledges support from the United States Department of Energy, Office of High Energy Physics under Award Number DE-SC-0011726. TMD is supported by an Australian Research Council Laureate Fellowship (project number FL180100168).

We acknowledge parts of this research were carried out on the traditional lands of the Ngunnawal and Ngambri peoples. This work makes use of data acquired at the Anglo-Australian Telescope, under program A/2013B/012. We acknowledge the Gamilaraay people as

the traditional owners of the land on which the AAT stands. We pay our respects to their elders past, present, and emerging.

This analysis used NUMPY (Harris et al. 2020), ASTROPY (Astropy Collaboration et al. 2013, 2018), and SCIPLY (Virtanen et al. 2020). Plots were made using MATPLOTLIB (Hunter 2007). This work has made use of the SAO/NASA Astrophysics Data System Bibliographic Services.

This paper has gone through internal review by the DES collaboration. Funding for the DES Projects has been provided by the U.S. Department of Energy, the U.S. National Science Foundation, the Ministry of Science and Education of Spain, the Science and Technology Facilities Council of the United Kingdom, the Higher Education Funding Council for England, The National Center for Supercomputing Applications at the University of Illinois at Urbana-Champaign, the Kavli Institute for Cosmological Physics at the University of Chicago, the Center for Cosmology and AstroParticle Physics at the Ohio State University, the Mitchell Institute for Fundamental Physics and Astronomy at Texas A&M University, Financiadora de Estudos e Projetos, Fundação Carlos Chagas Filho de Amparo à Pesquisa do Estado do Rio de Janeiro, Conselho Nacional de Desenvolvimento Científico e Tecnológico and the Ministério da Ciência, Tecnologia e Inovação, the Deutsche Forschungsgemeinschaft and the Collaborating Institutions in the Dark Energy Survey.

The Collaborating Institutions are Argonne National Laboratory, the University of California at Santa Cruz, the University of Cambridge, Centro de Investigaciones Energéticas, Medioambientales y Tecnológicas-Madrid, the University of Chicago, University College London, the DES-Brazil Consortium, the University of Edinburgh, the Eidgenössische Technische Hochschule (ETH) Zürich, Fermi National Accelerator Laboratory, the University of Illinois at Urbana-Champaign, the Institut de Ciències de l'Espai (IEEC/CSIC), the Institut de Física d'Altes Energies, Lawrence Berkeley National Laboratory, the Ludwig-Maximilians Universität München and the associated Excellence Cluster Universe, the University of Michigan, NSF's NOIRLab, the University of Nottingham, The Ohio State University, the University of Pennsylvania, the University of Portsmouth, SLAC National Accelerator Laboratory, Stanford University, the University of Sussex, Texas A&M University, and the OzDES Membership Consortium.

Based in part on observations at Cerro Tololo Inter-American Observatory at NSF's NOIRLab (NOIRLab Prop. ID 2012B-0001; PI: J. Frieman), which is managed by the Association of Universities for Research in Astronomy (AURA) under a cooperative agreement with the National Science Foundation.

The DES data management system is supported by the National Science Foundation under Grant Numbers AST-1138766 and AST-1536171. The DES participants from Spanish institutions are partially supported by MICINN under grants ESP2017-89838, PGC2018-094773, PGC2018-102021, SEV-2016-0588, SEV-2016-0597, and MDM-2015-0509, some of which include ERDF funds from the European Union. IFAE is partially funded by the CERCA program of the Generalitat de Catalunya. Research leading to these results has received funding from the European Research Council under the European Union's Seventh Framework Program (FP7/2007-2013) including ERC grant agreements 240672, 291329, and 306478. We acknowledge support from the Brazilian Instituto Nacional de Ciência e Tecnologia (INCT) do e-Universo (CNPq grant 465376/2014-2).

This manuscript has been authored by Fermi Research Alliance, LLC under Contract No. DE-AC02-07CH11359 with the U.S. Department of Energy, Office of Science, Office of High Energy Physics.

**DATA AVAILABILITY**

Machine-readable light curves for the eight AGN in the final sample are available in the online supplementary material. The underlying DES and OzDES data are available in Abbott et al. (2021) and Lidman et al. (2020).

**REFERENCES**

- Abbott T. M. C. et al., 2021, *ApJS*, 255, 20  
 Astropy Collaboration et al., 2013, *A&A*, 558, A33  
 Astropy Collaboration et al., 2018, *AJ*, 156, 123  
 Barth A. J. et al., 2013, *ApJ*, 769, 128  
 Bentz M. C., Peterson B. M., Netzer H., Pogge R. W., Vestergaard M., 2009, *ApJ*, 697, 160  
 Bentz M. C. et al., 2010, *ApJ*, 720, L46  
 Bentz M. C. et al., 2013, *ApJ*, 767, 149  
 Bentz M. C. et al., 2014, *ApJ*, 796, 8  
 Bentz M. C., Cackett E. M., Crenshaw D. M., Horne K., Street R., Ou-Yang B., 2016a, *ApJ*, 830, 136  
 Bentz M. C. et al., 2016b, *ApJ*, 831, 2  
 Blandford R. D., McKee C. F., 1982, *ApJ*, 255, 419  
 Burke D. L. et al., 2018, *AJ*, 155, 41  
 Childress M. J. et al., 2017, *MNRAS*, 472, 273  
 Du P. et al., 2014, *ApJ*, 782, 45  
 Du P. et al., 2015, *ApJ*, 806, 22  
 Du P. et al., 2016, *ApJ*, 825, 126  
 Du P. et al., 2018, *ApJ*, 856, 6  
 Fausnaugh M. M. et al., 2017, *ApJ*, 840, 97  
 Ferrarese L., Merritt D., 2000, *ApJ*, 539, L9  
 Flaugher B. et al., 2015, *AJ*, 150, 150  
 Fonseca Alvarez G. et al., 2020, *ApJ*, 899, 73  
 Gaskell C. M., Peterson B. M., 1987, *ApJS*, 65, 1  
 Gebhardt K. et al., 2000, *ApJ*, 543, L5  
 Gravity Collaboration et al., 2018, *Nature*, 563, 657  
 Grier C. J. et al., 2013, *ApJ*, 764, 47  
 Grier C. J. et al., 2017, *ApJ*, 851, 21  
 Grier C. J. et al., 2019, *ApJ*, 887, 38  
 Harris C. R. et al., 2020, *Nature*, 585, 357  
 Homayouni Y. et al., 2020, *ApJ*, 901, 55  
 Hoormann J. K. et al., 2019, *MNRAS*, 487, 3650  
 Hu C. et al., 2021, *ApJS*, 253, 20  
 Hunter J. D., 2007, *Comput. Sci. Eng.*, 9, 90  
 Kaspi S., Smith P. S., Netzer H., Maoz D., Jannuzi B. T., Giveon U., 2000, *ApJ*, 533, 631  
 Kelly B. C., Bechtold J., Siemiginowska A., 2009, *ApJ*, 698, 895  
 Kessler R. et al., 2015, *AJ*, 150, 172  
 Khadka N., Martínez-Aldama M. L., Zajaček M., Czerny B., Ratra B., 2022, *MNRAS*, 513, 1985  
 King A. L. et al., 2015, *MNRAS*, 453, 1701  
 Kollmeier J. A. et al., 2017, preprint (arXiv:1711.03234)  
 Kozłowski S. et al., 2010, *ApJ*, 708, 927  
 Li J. I.-H. et al., 2019, *ApJ*, 884, 119  
 Li S.-S. et al., 2021, *ApJ*, 920, 9  
 Lidman C. et al., 2020, *MNRAS*, 496, 19  
 Lu K.-X. et al., 2016, *ApJ*, 827, 118  
 MacLeod C. L. et al., 2010, *ApJ*, 721, 1014  
 Malik U. et al., 2022, *MNRAS*, 516, 3238  
 Martínez-Aldama M. L., Czerny B., Kawka D., Karas V., Panda S., Zajaček M., Życki P. T., 2019, *ApJ*, 883, 170  
 Morganson E. et al., 2018, *PASP*, 130, 074501  
 Onken C. A., Ferrarese L., Merritt D., Peterson B. M., Pogge R. W., Vestergaard M., Wandel A., 2004, *ApJ*, 615, 645  
 Pancoast A., Brewer B. J., Treu T., 2014a, *MNRAS*, 445, 3055  
 Pancoast A., Brewer B. J., Treu T., Park D., Barth A. J., Bentz M. C., Woo J.-H., 2014b, *MNRAS*, 445, 3073  
 Pei L. et al., 2014, *ApJ*, 795, 38  
 Penton A. et al., 2022, *MNRAS*, 509, 4008  
 Peterson B. M., 1993, *PASP*, 105, 247  
 Peterson B. M., Horne K., 2004, *Astron. Nachr.*, 325, 248  
 Peterson B. M., Wanders I., Horne K., Collier S., Alexander T., Kaspi S., Maoz D., 1998, *PASP*, 110, 660  
 Rakshit S. et al., 2019, *ApJ*, 886, 93  
 Shakura N. I., Sunyaev R. A., 1973, *A&A*, 24, 337  
 Sharp R. et al., 2006, in McLean I. S., Iye M., eds, Proceedings Volume 6269, Ground-based and Airborne Instrumentation for Astronomy; 6269G (2006) Event: SPIE Astronomical Telescopes + Instrumentation, 2006, Orlando, Florida, United States. Society of Photo-Optical Instrumentation Engineers (SPIE), Bellingham, Washington USA, p. 62690G  
 Shen Y., 2013, *Bull. Astron. Soc. India*, 41, 61  
 Shen Y. et al., 2011, *ApJS*, 194, 45  
 Shen Y. et al., 2015, *ApJS*, 216, 4  
 Sun M., Grier C. J., Peterson B. M., 2018, Astrophysics Source Code Library, record ascl:1805.032, PyCCF: Python Cross Correlation Function for reverberation mapping studies  
 Swann E. et al., 2019, *The Messenger*, 175, 58  
 U V. et al., 2022, *ApJ*, 925, 52  
 Vanden Berk D. E. et al., 2001, *AJ*, 122, 549  
 Vestergaard M., 2002, *ApJ*, 571, 733  
 Vestergaard M., Peterson B. M., 2006, *ApJ*, 641, 689  
 Virtanen P. et al., 2020, *Nature Methods*, 17, 261  
 Wang J.-M. et al., 2014, *ApJ*, 793, 108  
 Watson D., Denney K. D., Vestergaard M., Davis T. M., 2011, *ApJ*, 740, L49  
 Woo J.-H., Yoon Y., Park S., Park D., Kim S. C., 2015, *ApJ*, 801, 38  
 Yu Z., Kochanek C. S., Peterson B. M., Zu Y., Brandt W. N., Cackett E. M., Fausnaugh M. M., McHardy I. M., 2020, *MNRAS*, 491, 6045  
 Yu Z. et al., 2021, *MNRAS*, 507, 3771  
 Yu Z. et al., 2022, preprint (arXiv:2208.05491)  
 Yuan F. et al., 2015, *MNRAS*, 452, 3047  
 Zhang Z.-X. et al., 2019, *ApJ*, 876, 49  
 Zu Y., Kochanek C. S., Peterson B. M., 2011, *ApJ*, 735, 80  
 Zu Y., Kochanek C. S., Kozłowski S., Udalski A., 2013, *ApJ*, 765, 106

**SUPPORTING INFORMATION**

Supplementary data are available at *MNRAS* online.

**Hbeta.lightcurves.zip**

Please note: Oxford University Press is not responsible for the content or functionality of any supporting materials supplied by the authors. Any queries (other than missing material) should be directed to the corresponding author for the article.

**APPENDIX A: SOURCES WITH JAVELIN ALIASING**

Here we include additional figures referenced in Section 4.1. Figs A1 and A2 show the light curves and lag PDF's for the five of the eight sources with JAVELIN aliasing signals that we do not include on our final sample. Although two of these sources do pass our selection criteria after omitting the negative JAVELIN aliasing peak, we choose to not include them in our final sample as the positive lag is not constrained by overlap between the photometric and spectroscopic data. We show the light curves phase-shifted by both the positive lag and the negative lag in Fig. A3 for the three sources which are included in our final sample, and in Fig. A4 for the other five sources.

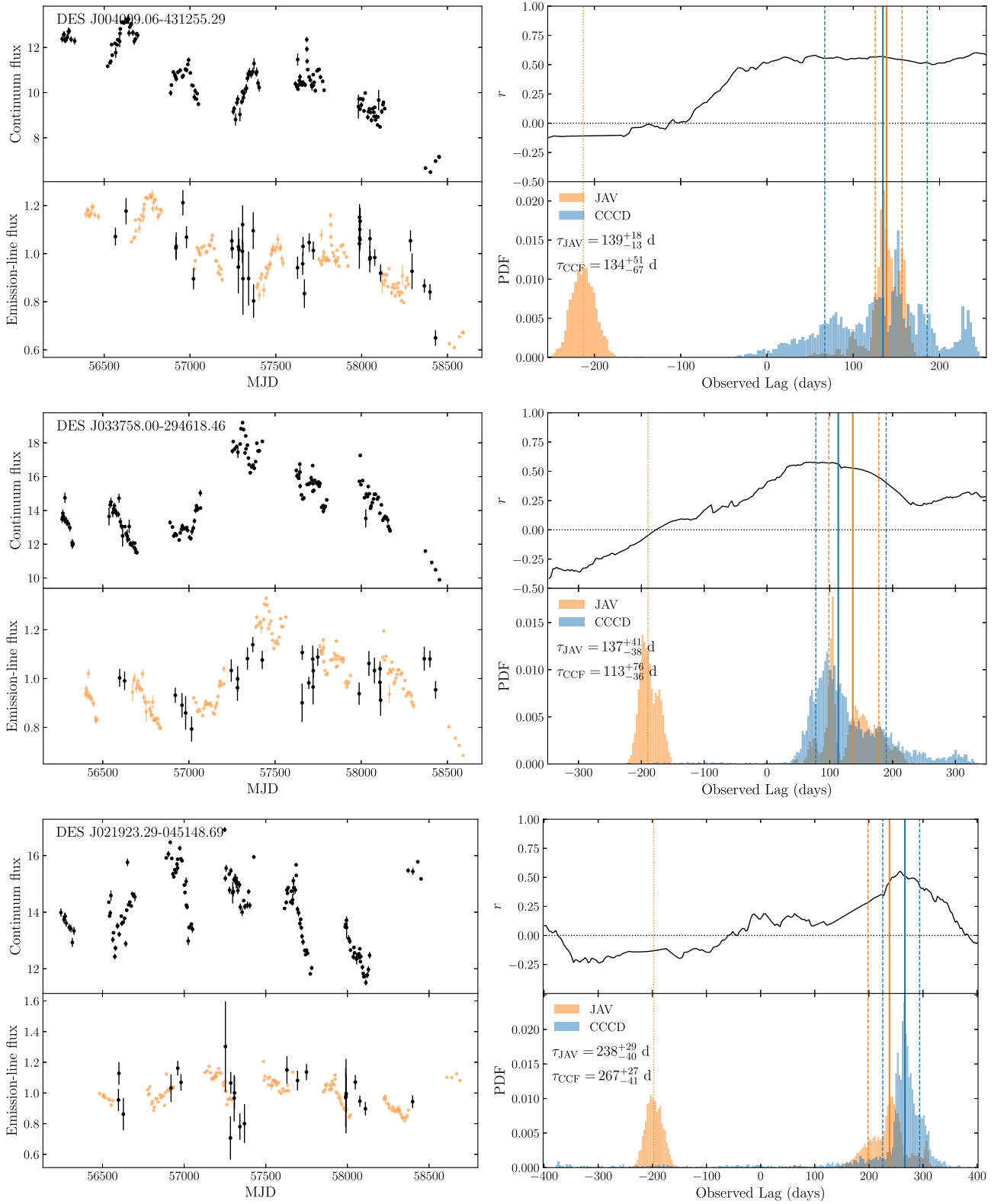
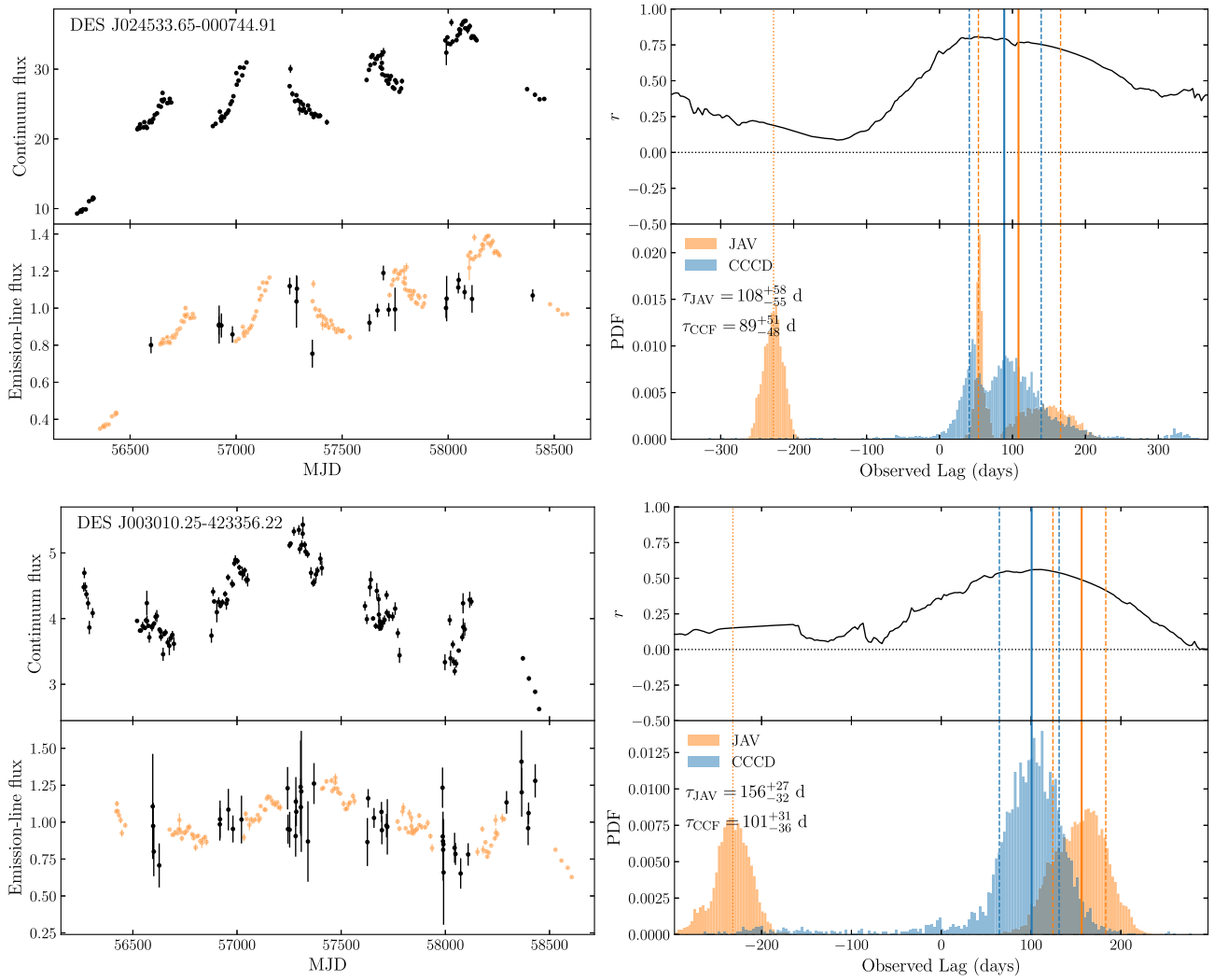
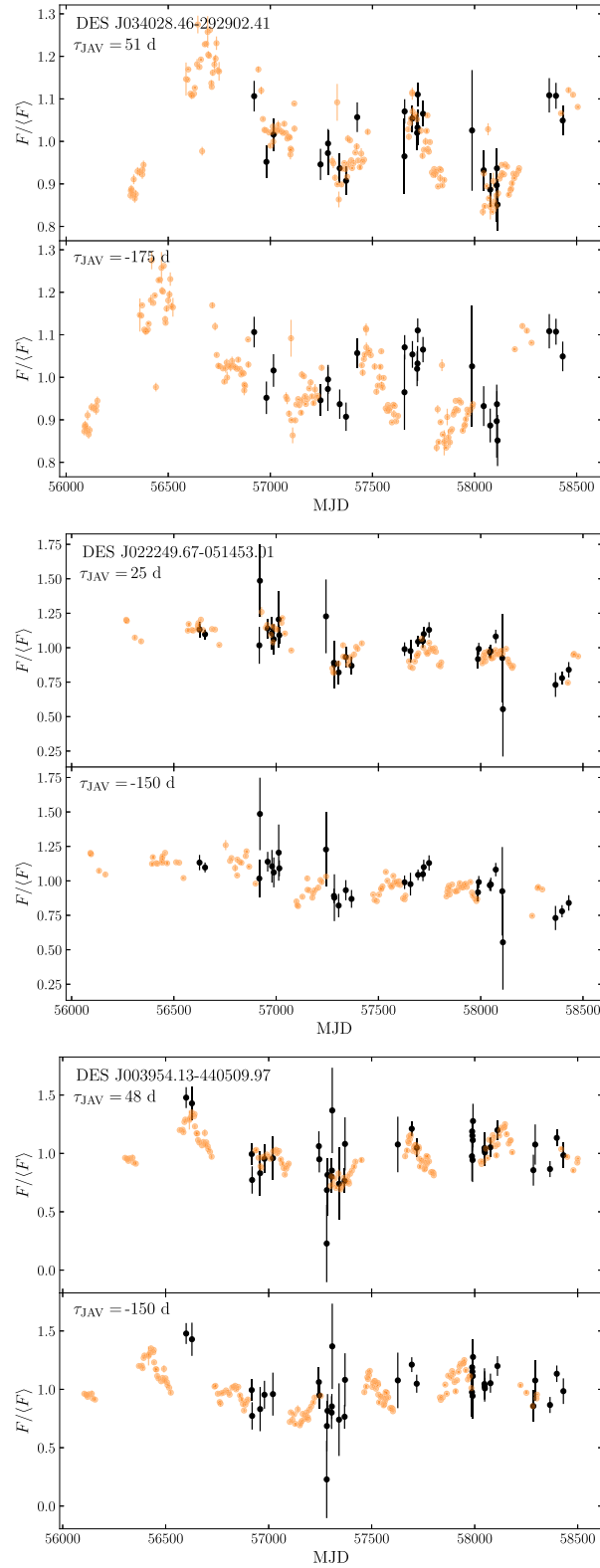


Figure A1. Same as for Fig. 6. These sources are not included in the final sample.



**Figure A2.** Same as for Fig. 6. These sources are not included in the final sample.



**Figure A3.** The emission-line light curve (black) and phase-shifted continuum light curve (orange) for the additional three sources we include in our final sample. The top and bottom panels show the continuum shifted by the positive and negative lag, respectively. For each source there is overlap between the light curves phase-shifted by the positive lag, while the negative lag shifts the continuum light curves wholly within the seasonal gaps of the emission-line light curve.

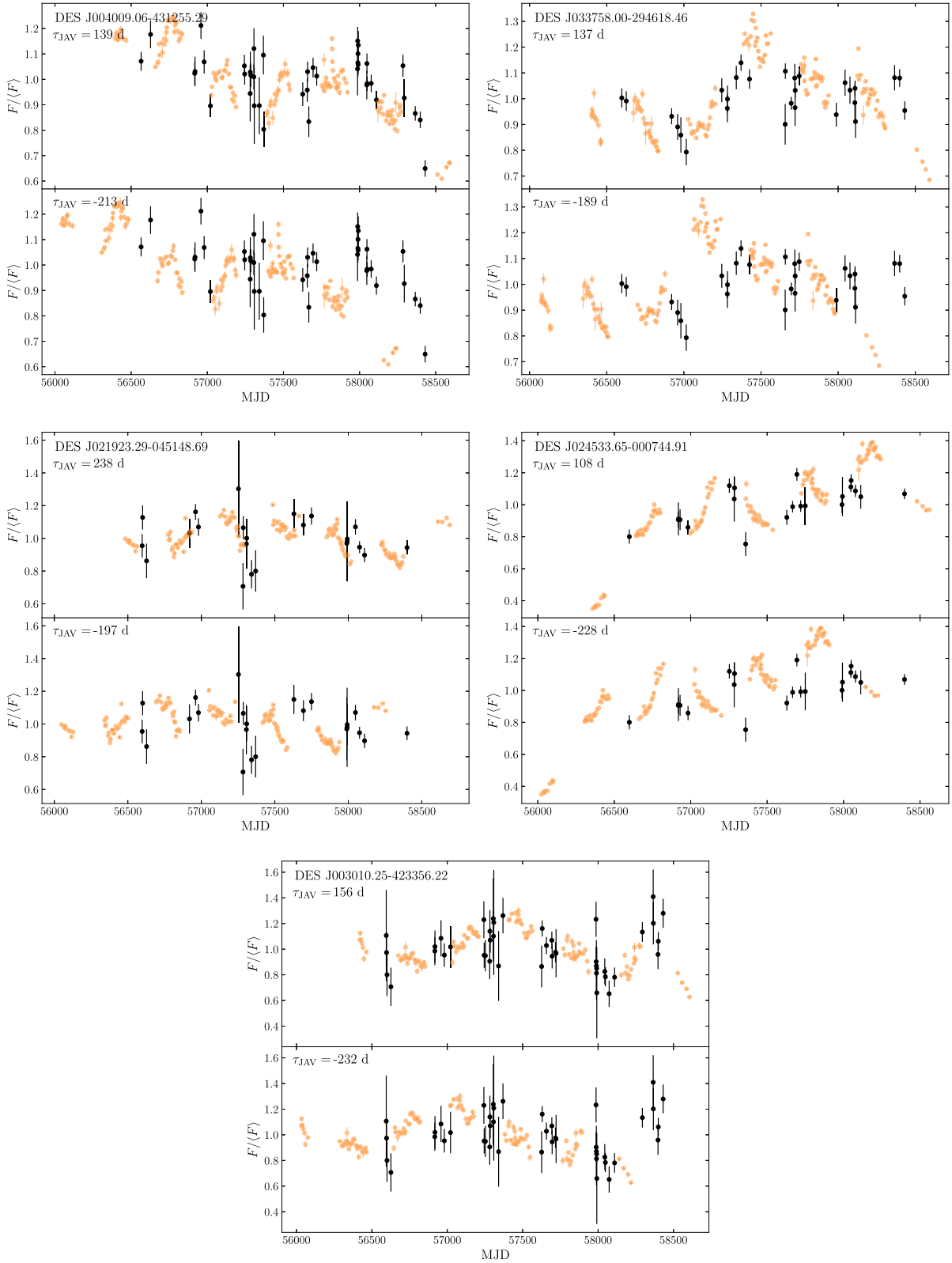


**Figure A4.** The emission-line light curve (black) and phase-shifted continuum light curve (orange) for the five sources in Fig. A1 and Fig. A2, which we do not include in our final sample. The top and bottom panels show the continuum shifted by the positive and negative lag, respectively. For each source, in both cases there is no overlap between the photometric and spectroscopic observations.

- <sup>1</sup>Research School of Astronomy and Astrophysics, Australian National University, Canberra, ACT 2611, Australia
- <sup>2</sup>School of Mathematics and Physics, The University of Queensland, St Lucia, QLD 4101, Australia
- <sup>3</sup>Department of Astronomy, The Ohio State University, Columbus, Ohio 43210, USA
- <sup>4</sup>Center of Cosmology and Astro-Particle Physics, The Ohio State University, Columbus, Ohio 43210, USA
- <sup>5</sup>Radcliffe Institute for Advanced Study, Harvard University, Cambridge, MA 02138, USA
- <sup>6</sup>National Centre for the Public Awareness of Science, Australian National University, Canberra, ACT 2601, Australia
- <sup>7</sup>The Australian Research Council Centre of Excellence for All-Sky Astrophysics in 3 Dimension (ASTRO 3D), Australia
- <sup>8</sup>Sydney Institute for Astronomy, School of Physics, A28, The University of Sydney, Sydney, NSW 2006, Australia
- <sup>9</sup>Laboratório Interinstitucional de e-Astronomia - LIneA, Rua Gal. José Cristino 77, Rio de Janeiro, RJ - 20921-400, Brazil
- <sup>10</sup>Fermi National Accelerator Laboratory, P. O. Box 500, Batavia, IL 60510, USA
- <sup>11</sup>Department of Physics, University of Michigan, Ann Arbor, MI 48109, USA
- <sup>12</sup>Centro de Investigaciones Energéticas, Medioambientales y Tecnológicas (CIEMAT), Madrid, Spain
- <sup>13</sup>Institute of Cosmology and Gravitation, University of Portsmouth, Portsmouth, PO1 3FX, UK
- <sup>14</sup>CNRS, UMR 7095, Institut d'Astrophysique de Paris, F-75014, Paris, France
- <sup>15</sup>Sorbonne Universités, UPMC Univ Paris 06, UMR 7095, Institut d'Astrophysique de Paris, F-75014, Paris, France
- <sup>16</sup>University Observatory, Faculty of Physics, Ludwig-Maximilians-Universität, Scheinerstr. 1, D-81679 Munich, Germany
- <sup>17</sup>Department of Physics & Astronomy, University College London, Gower Street, London, WC1E 6BT, UK
- <sup>18</sup>Kavli Institute for Particle Astrophysics & Cosmology, P. O. Box 2450, Stanford University, Stanford, CA 94305, USA
- <sup>19</sup>SLAC National Accelerator Laboratory, Menlo Park, CA 94025, USA
- <sup>20</sup>Instituto de Astrofísica de Canarias, E-38205 La Laguna, Tenerife, Spain
- <sup>21</sup>Universidad de La Laguna, Dpto. Astrofísica, E-38206 La Laguna, Tenerife, Spain
- <sup>22</sup>INAF-Osservatorio Astronomico di Trieste, via G. B. Tiepolo 11, I-34143 Trieste, Italy
- <sup>23</sup>Department of Astronomy, University of Illinois at Urbana-Champaign, 1002 W. Green Street, Urbana, IL 61801, USA
- <sup>24</sup>Center for Astrophysical Surveys, National Center for Supercomputing Applications, 1205 West Clark St., Urbana, IL 61801, USA
- <sup>25</sup>Institut de Física d'Altes Energies (IFAE), The Barcelona Institute of Science and Technology, Campus UAB, 08193 Bellaterra (Barcelona) Spain
- <sup>26</sup>Institute for Fundamental Physics of the Universe, Via Beirut 2, 34014 Trieste, Italy
- <sup>27</sup>Astronomy Unit, Department of Physics, University of Trieste, via Tiepolo 11, I-34131 Trieste, Italy
- <sup>28</sup>Hamburger Sternwarte, Universität Hamburg, Gojenbergsweg 112, D-21029 Hamburg, Germany
- <sup>29</sup>Department of Physics, IIT Hyderabad, Kandi, Telangana 502285, India
- <sup>30</sup>Jet Propulsion Laboratory, California Institute of Technology, 4800 Oak Grove Dr., Pasadena, CA 91109, USA
- <sup>31</sup>Institute of Theoretical Astrophysics, University of Oslo. P.O. Box 1029 Blindern, NO-0315 Oslo, Norway
- <sup>32</sup>Kavli Institute for Cosmological Physics, University of Chicago, Chicago, IL 60637, USA
- <sup>33</sup>Instituto de Física Teórica UAM/CSIC, Universidad Autónoma de Madrid, E-28049 Madrid, Spain
- <sup>34</sup>Department of Astronomy, University of Michigan, Ann Arbor, MI 48109, USA
- <sup>35</sup>Observatório Nacional, Rua Gal. José Cristino 77, Rio de Janeiro, RJ - 20921-400, Brazil
- <sup>36</sup>Santa Cruz Institute for Particle Physics, Santa Cruz, CA 95064, USA
- <sup>37</sup>Center for Astrophysics | Harvard & Smithsonian, 60 Garden Street, Cambridge, MA 02138, USA
- <sup>38</sup>Australian Astronomical Optics, Macquarie University, North Ryde, NSW 2113, Australia
- <sup>39</sup>Lowell Observatory, 1400 Mars Hill Rd, Flagstaff, AZ 86001, USA
- <sup>40</sup>George P. and Cynthia Woods Mitchell Institute for Fundamental Physics and Astronomy, and Department of Physics and Astronomy, Texas A&M University, College Station, TX 77843, USA
- <sup>41</sup>Institució Catalana de Recerca i Estudis Avançats, E-08010 Barcelona, Spain
- <sup>42</sup>Department of Astronomy, University of California, Berkeley, 501 Campbell Hall, Berkeley, CA 94720, USA
- <sup>43</sup>Institute of Astronomy, University of Cambridge, Madingley Road, Cambridge CB3 0HA, UK
- <sup>44</sup>Laboratório Interinstitucional de e-Astronomia - LIneA, Rua Gal. José Cristino 77, Rio de Janeiro, RJ - 20921-400, Brazil
- <sup>45</sup>Department of Astrophysical Sciences, Princeton University, Peyton Hall, Princeton, NJ 08544, USA
- <sup>46</sup>Department of Physics and Astronomy, University of Pennsylvania, Philadelphia, PA 19104, USA
- <sup>47</sup>Department of Physics and Astronomy, Pevensey Building, University of Sussex, Brighton, BN1 9QH, UK
- <sup>48</sup>School of Physics and Astronomy, University of Southampton, Southampton, SO17 1BJ, UK
- <sup>49</sup>Computer Science and Mathematics Division, Oak Ridge National Laboratory, Oak Ridge, TN 37831
- <sup>50</sup>Lawrence Berkeley National Laboratory, 1 Cyclotron Road, Berkeley, CA 94720, USA

This paper has been typeset from a  $\text{\TeX}/\text{\LaTeX}$  file prepared by the author.